J Mater Sci (2007) 42:1251–1260
DOI 10.1007/s10853-006-1382-z

The relationship between fracture toughness and microstructure of fully lamellar TiAl alloy

R. T. Zheng · G. A. Cheng · X. J. Li · G. X. CAO · L. F. Fu · Y. G. Zhang · C. Q. Chen

Received: 16 August 2004 / Accepted: 30 January 2006 / Published online: 21 January 2007

Abstract Fully lamellar (FL) Ti–46.5Al–2Cr–1.5Nb–1V (at%) alloy is used to study the relationship between microstructure and fracture toughness. A heat treatment process is adopted to control the microstructural parameters of the studied alloy. Fracture toughness experiments and scanning electron microscope (SEM) in-situ straining experiments are carried out to determine the influence of lamellar spacing and grain size on the fracture toughness of FL TiAl alloys. It is found that ligament length depends on the lamellar spacing, and fracture toughness varies non-monotonously with the increase of grain size. The results are ascribed to the competition between the microcrack nucleation and microcrack propagation. Finally a semi-empirical relationship between the fracture toughness and microstructure parameters was established.

Introduction

Gamma TiAl alloys are promising candidates for high-temperature applications in automotive and aerospace industry because of their low density, good elevated-temperature strength, high resistance to oxidation and excellent creep properties. It is widely accepted that the mechanical properties of two-phase TiAl alloys strongly depend on their microstructures [1–5]. In the four types of microstructures of γ-TiAl alloys, which include near gamma (NG), duplex (DP), nearly lamellar (NL) and fully lamellar (FL), the fully lamellar microstructure is the most attractive because of its overall balance of properties. Though its ambient ductility is relatively low, FL TiAl alloys have higher yield strength, fracture toughness and creep resistance, and are more suitable for high-temperature application than DP or NG TiAl alloys [6–8].

At ambient temperature, the fracture toughness of the fully lamellar polycrystalline alloys ranges from 20 to 30 MPa $m^{1/2}$, and is about twice that of the alloys with duplex and near gamma microstructure[9, 10]. The fracture behavior of FL TiAl alloys has been studied extensively in the last two decades. Research efforts demonstrated that FL TiAl based alloys are generally more resistant to fracture than those with either the NG or DP microstructure and the reason has been suggested to be the formation of intact ligaments between the main crack and the microcracks[11–13]. It has been fully realized that both grain size and lamellar spacing have strong influence on the fracture process of FL TiAl alloys. The crack path in FL TiAl alloys has been studied in a number of investigations [13–16], and the effect of microstructural parameters on the crack path and fracture ligaments has been investigated [8, 10, 14, 17–20], as a result, the relationship between grain size or lamellar spacing and fracture toughness of FL TiAl alloys has been established. But the results are unclear because grain size and lamellar spacing were

R. T. Zheng (✉) · G. A. Cheng · X. J. Li
Key Laboratory of Radiation Beam Technology and Materials Modification of Ministry of Education, Institute of Low Energy Nuclear Physics, Beijing Normal University, Beijing 100875, China
e-mail: ruiting_zheng@yahoo.com.cn

G. X. CAO · L. F. Fu · Y. G. Zhang · C. Q. Chen
Department of Materials Science and Engineering, Beijing University of Aeronautics & Astronautics, Beijing 100083, China

changed simultaneously in these studies. It is necessary to control the microstructure and then to systematically study the effects of microstructure parameters on the fracture toughness of FL TiAl alloys.

The purpose of this work is to determine the relationships between grain size, lamellar spacing and the fracture toughness of FL TiAl alloys by considering the toughening effects of fracture ligaments. In order to achieve this goal, a controlled heat treatment process [21] was employed to separate these two microstructure parameters. Then fracture toughness tests and SEM in-situ straining experiments were carried out. Based on the experimental investigation and theoretical analysis, a model is established to describe the relationship between microstructure and fracture toughness of FL TiAl alloys.

Experimental

Materials

The alloy with a nominal composition of Ti–46.5Al–2Cr–1.5Nb–1V (at.%) was prepared using a cold crucible induction furnace. The obtained ingots (approximately 30 mm in diameter and 250 mm in length) were hot isostatically pressed (HIP) (1260 °C, 175 MPa/3 h) in an argon atmosphere to seal casting porosity. Samples were cut from the ingot and prepared for heat treatment by wrapping in Ta foil and sealing in quartz tubes back-filled with argon to 3000 Pa.

Microstructures

According to our previous study [21], two heat treatment processes were designed to obtain two series of FL TiAl alloys. One had identical lamellar spacing but different grain size; and the other had identical grain size but different lamellar spacing. The details of the samples and their heat treatments are listed in Table 1. The average grain sizes of the samples tested in this study were determined using NEOPHOT-2 optical microscopes and the line-intercept method. Mean lamellar spacing was measured using a H-800 transmission electron microscope (TEM). The thin foil samples were oriented in such a way so that the lamellar plates were parallel to the electron beam, and the lamellar spacing was measured at least in three grains for each of the samples. The lamellar spacing (λ) was defined as the edge-to-edge dimension (measured perpendicular to the interface boundary) without regarding the phase type of the lamellae.

Table 1 Heat treatment processes, microstructure parameters and fracture toughness of samples

Samples	Heat treatment processes	Microstructure parameters		Average Fracture toughness ($MPam^{1/2}$)
		Grain size (μm)	Lamellar spacing (nm)	
a	1330 °C/4 min/ FC(60 °C/min)	260	170	25.3
b	1330 °C/5 min/ FC(60 °C/min)	300	155	27.6
c	1330 °C/6 min/ FC(60 °C/min)	355	162	26.2
d	1330 °C/7 min/ FC(60 °C/min)	400	156	26.6
e	1330 °C/10 min/ FC(60 °C/min)	600	160	30.8
f	1330 °C/12 min/ FC(60 °C/min)	700	168	30.2
g	1330 °C/15 min/ FC(60 °C/min)	800	170	28.3
h	1330 °C/30 min/ FC(60 °C/min)	1250	174	21.1
i	1320 °C/8 min/ AC(100 °C/min)	380	95	29.3
j	1320 °C/8 min/ FC(60 °C/min)	375	160	28.1
k	1320 °C/8 min/ FC(10 °C/min)	360	300	26.6
l	1320 °C/8 min/ FC(3 °C/min)	390	650	25.45

Mechanical testing

Standard ASTM plane-strain (Chevron-Notch) specimens [22], 10.5 mm wide, 10.5 mm high and 16.3 mm long, were prepared for testing fracture toughness. In this study, the value for K_{IVM} was tested as fracture toughness of the samples. At least three samples were tested for each microstructure condition, and the mean K_{IVM} is reported.

In-situ straining experiments

Specimens for in-situ straining experiments with a length of 15 mm and cross section of 5×1.5 mm^2 were cut from the ingots with different microstructures using an electric discharge machine, followed by grinding and electro-polishing to eliminate the surface damage. Finally, they were fatigue-precracked. The in-situ straining experiments were conduced in a JSM-5800 scanning electron microscope equipped with a JEOL tensile stage, and the specimens were loaded manually. The microcrack nucleation and crack path were observed and recorded using both secondary electron imaging and backscatter electron imaging.

Results

Microstructures and fracture toughness

Figure 1 shows micrographs taken from samples (a–h) which have similar lamellar spacing (160 nm), but different grain size. The average grain size was measured for each of the samples and the results are listed in Table 1. TEM micrographs taken from samples (i–l) with different lamellar spacing are shown in Fig. 2. Grain size of these four samples was controlled to be the same (375 μm). The heat treatment processes, microstructure parameters and fracture toughness of the samples tested in this work are all presented in Table 1.

Based on the microstructural control, the relationship between the fracture toughness and the microstructural parameters has been studied, as shown in Fig. 3. The curve in Fig. 3(a) is a polynomial fit of experimental data. It can be seen that the fracture toughness increases with the increase of the grain size in the smaller grain size range, reaches a peak value at the grain size of 600~700μm, and then decreases with the further increase of grain size. The relationship between the fracture toughness and lamellar spacing is relatively simple. It increases with the decrease of

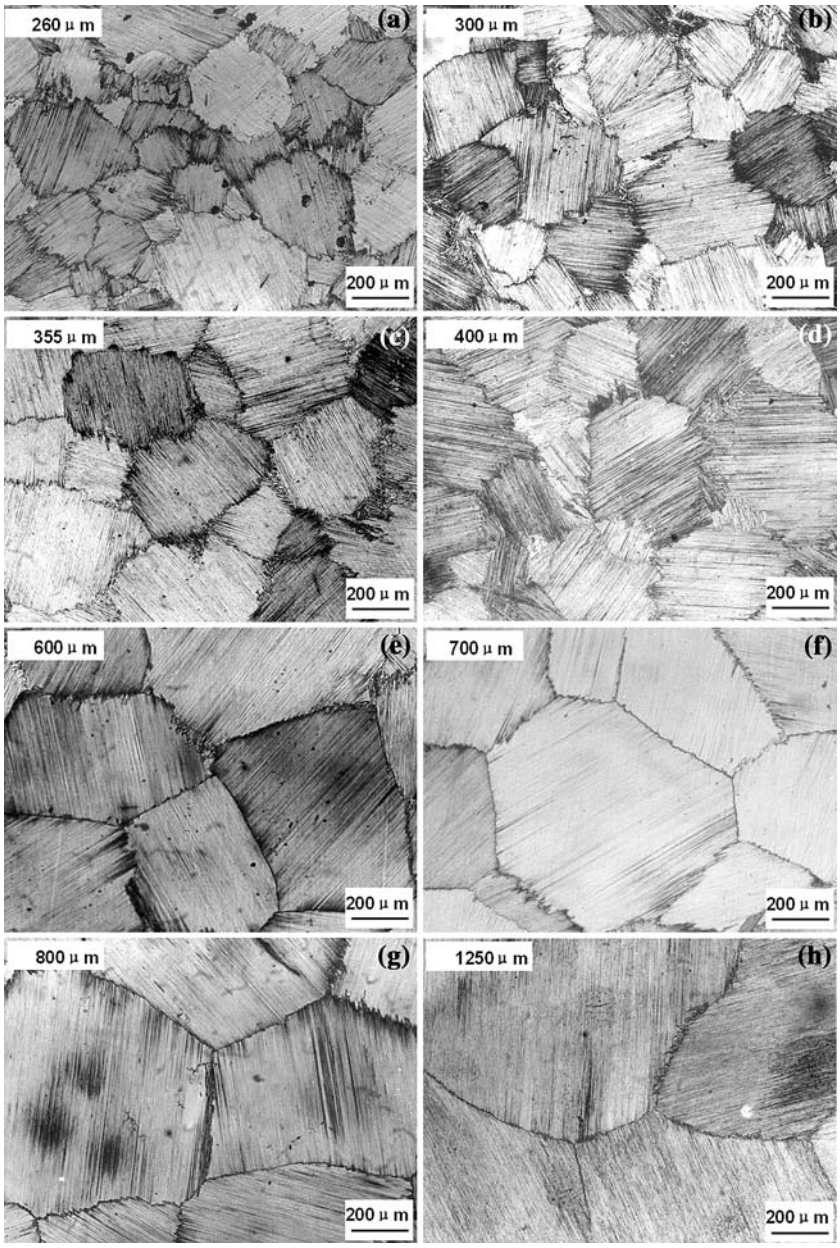

Fig. 1 Metallographs of the fully lamellar TiAl alloy with about 160 nm of lamellar spacing and different grain size

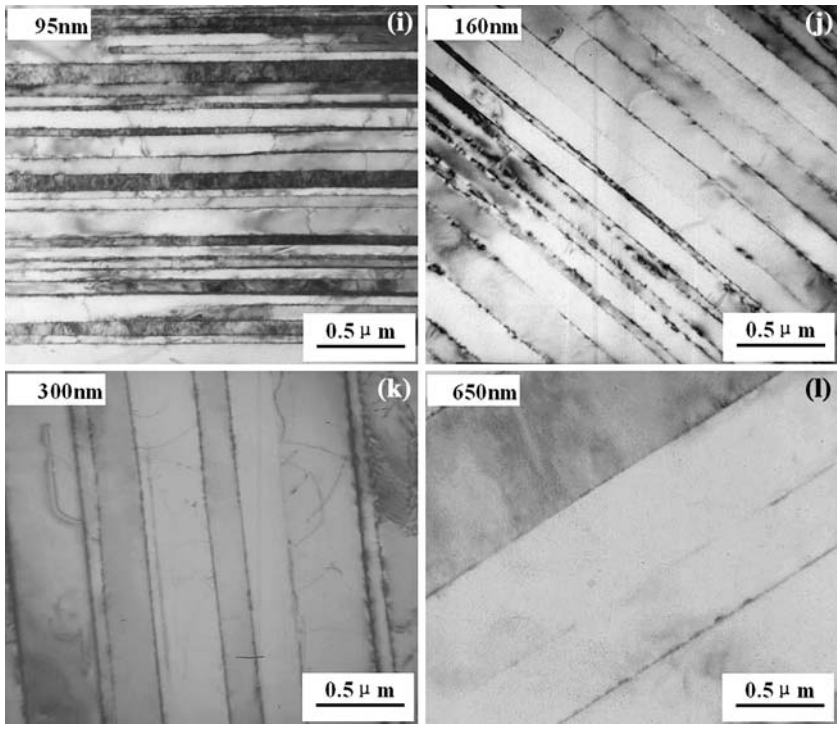

Fig. 2 TEM micrographs of fully lamellar TiAl alloy with about 375 μm of grain size and different lamellar spacing

lamellar spacing, and satisfies Hall–Petch relationship, as shown in Fig. 3b.

In-situ observation of microcracks

Figure 4 shows typical secondary electron images of crack paths on the surface of in-situ straining specimens with microstructures (a) and (g). When grain size is relatively small, the main crack tends to propagate along or across the lamellar interface and grain boundary (it depends on the location of crack tip). Since the grain size is small, lamellar orientation has little effect on the crack path and the crack path is relatively straight (Fig. 4a). In the specimen with large grain size, orientation of the crack path changed sharply when the crack transferred from one grain to another (Fig. 4b). As a result, the path of the main crack turned out to be tortuous and, therefore, longer. The relationship between the path of the main crack and grain size can be obtained by fitting the experimental data:

$$L_c = L_0(1 + 546.3D) \quad (1)$$

where L_0 is the projected length of the main crack path and D is the average diameter of grains.

It has been well known that FL TiAl alloys with smaller lamellar spacing have higher fracture toughness, but the toughening mechanism is not clear up to now. In order to find the influence of lamellar spacing on the fracture toughness, specimens with microstructures (j) and (l) were in-situ strained. In these samples, it is found that delamination is the main fracture mode, and the fracture mode does not change with the change of lamellar spacing. Ligament toughening is the most important extrinsic mechanism that enhances the apparent fracture resistance by reducing the near-tip crack driving force. The difference of fracture toughness between the samples with different lamellar spacing lies in the difference of ligament. In accordance with a previous report [13], it is found that the ligament length L, rather than ligament height H (as shown in Fig. 6) depends on the lamellar spacing. The specimen with smaller lamellar spacing has longer ligament, as shown in Fig. 5.

Analysis and discussion

Stress state of the ligament

In all extrinsic toughening mechanisms of γ-TiAl alloys, crack bridging by ligaments is the most important factor that leads to additional toughening. In order to specify the effect of ligament on the fracture toughness, the stress state of the ligament must be investigated.

It can be seen from Fig. 5 that a heavy bending deformation occurred in the ligament. The ligament

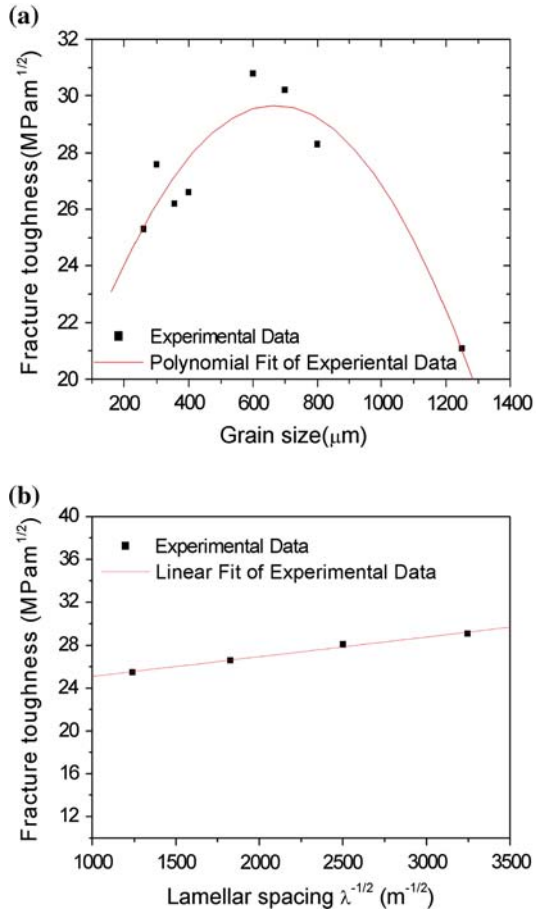

Fig. 3 The relationship between the microstructure and fracture toughness: (**a**) fracture toughness vs. grain size (lamellar spacing of the alloys is about 160 nm); (**b**) fracture toughness vs. lamellar spacing (grain size of the alloy is about 375 μm)

could be simplified as a beam with two ends fixed. With the application of an external load, a vertical displacement is generated between the two ends. Fig. 6 is the schematic drawing of deformation and stress state in the deformed ligament. It is a statically indeterminate problem. By replacing the two ends fixed beam with a cantilever beam with a bending movement and a shear stress applied on its right end, the problem is converted to a statical problem. With the addition of the boundary condition, i.e., the slope of the right end equals zero, the inner stress of the ligament can be obtained by materials mechanics.

The maximum normal stress :

$$\sigma_{\max} = \frac{M}{W_y} = PL/\frac{bH^2}{6} = \frac{6PL}{bH^2} \tag{2}$$

The shear stress :

$$\tau_{\max} = P/bH \tag{3}$$

where P is the shearing force applied on the right end of the cantilever beam. M is the movement applied on the right end of the cantilever beam, $M = PLW_y$ is elastic section modulus, L is the length of beam, b is the width of beam, and H is the height of beam.

Suppose $L = H$, we have $\sigma_{\max} = \frac{6P}{bH} = 6\tau$ from Eqs. (2) and (3). It is obvious that the normal stress is six times as large as the shear stress in the ligament, even if the length of ligament is as short as the height of it. So the main cause of the fracture of the ligament is not the shearing stress, but the bending and shearing stress. Therefore the concept of shear ligament is not complete, and bend and shear combined ligament would be a more accurate description.

Numerical relationship between lamellar spacing and ligament length

From the micro-deformation mechanism study of the deformed FL γ-TiAl alloys [23], it was found that

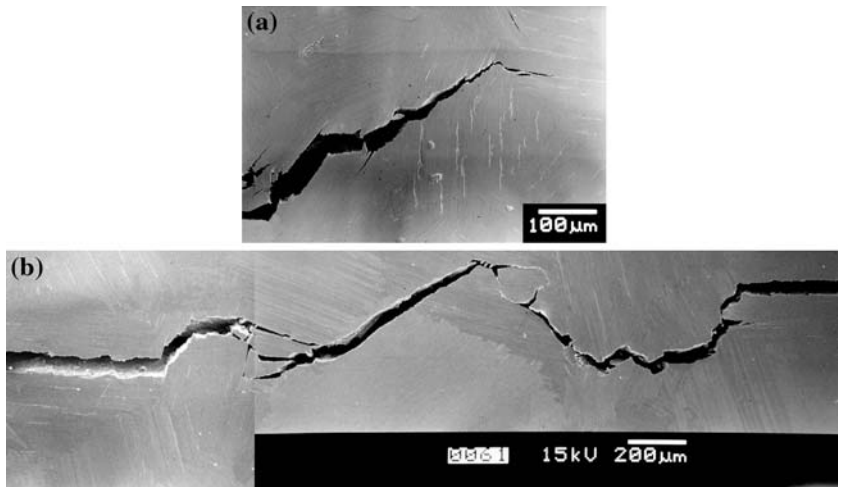

Fig. 4 The typical secondary electron images of crack path in TiAl alloy with different grain sizes and 170 nm of lamellar spacing: (**a**) grain size equals 260μm; (**b**) grain size equals 800μm

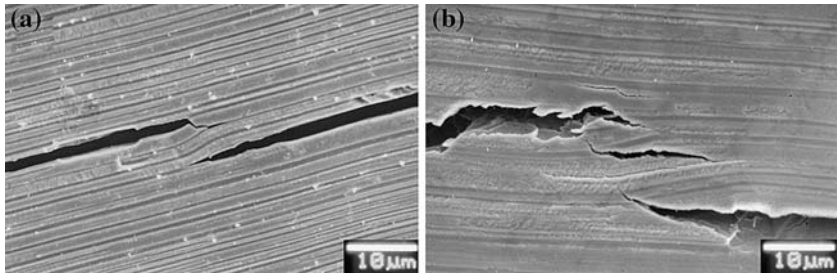

Fig. 5 The typical secondary electron images of ligament in TiAl alloy with different lamellar spacings and 380μm of grain size: (**a**) lamellar spacing equals 160 nm; (**b**) lamellar spacing equals 650 nm

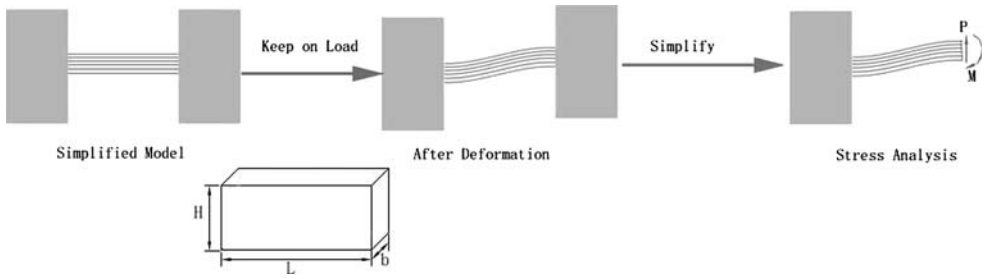

Fig. 6 The schematic diagram of stress state in ligament

1/2[110] ordinary dislocations and 1/6[112] twins are the main deformation mode at ambient temperature. And the major proportion of deformation in these alloys comes from the ordinary dislocation. There are two kinds of shearing deformation modes induced by the slip of ordinary dislocations, interlamellar shearing deformation and translamellar shearing deformation. These two deformation modes have the similar effects on the deformation of ligaments, as shown in Fig. 7. If the height of ligaments is almost the same, the ligaments with smaller lamellar spacing will have larger deformation.

Assuming the average shearing deformation (the sum of interlamellar and translamellar shearing deformation) of each lamellar interface is $\triangle d$, the average lamellar spacing is h (as shown in Fig. 7) and the height of ligament is H, then $H = nh$, in which n is the number of lamellae in the ligament.

Since the angle of the shearing deformation is small, it is given by:

$$\theta_s \approx tg\theta_s = \frac{n \times \Delta d}{H} = \frac{\Delta d}{h} \tag{4}$$

Suppose θ_s is generated by an equivalent bending movement M_s, and M_s satisfies the equation

$$\theta_s = \frac{M_s L}{EI} \tag{5}$$

where E is the elastic modulus, L is the length of ligament, and I is the moment of inertia.

Substituting Eq. (4) into Eq. (5) leads to :

$$M_s = \frac{EI\Delta d}{hL} \tag{6}$$

Because Δd is proportional to the ligament length L, it can be described as:

$$\Delta d = C_1 L \tag{7}$$

where C_1 is a material constant.

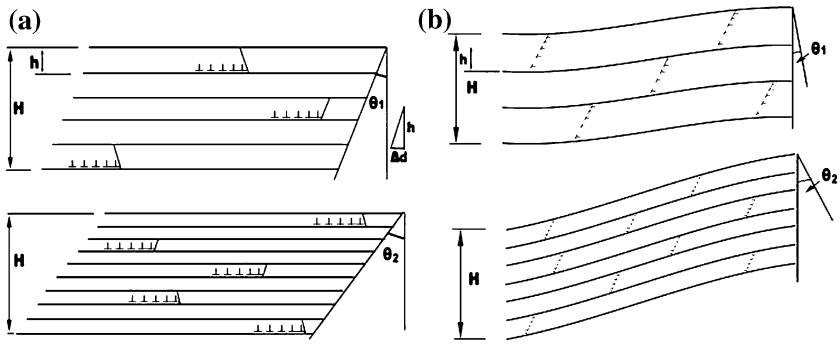

Fig. 7 The schematic diagram of deformation in ligament with different lamellar spacing: (**a**) interlamellar shearing; (**b**) translamellar shearing

Substituting Eq. (7) into Eq. (6) leads to :

$$M_s = \frac{EIC_1}{h} \tag{8}$$

The actual movement $M_{act} = M - M_s = PL - \frac{EIC_1}{h}$ (9)

As discussed in Section 'Stress state of the ligament', the bending stress is the main cause of ligament fracture, and the effect of shearing stress on the fracture of ligament can be neglected. So

$$\sigma_{frac} = \frac{M_{act}}{W_y} \tag{10}$$

Substituting Eq. (9) into Eq. (10), the ligament length can be expressed as:

$$L = \frac{W_y \cdot \sigma_{frac}}{P} + \frac{EIC_1}{Ph} \tag{11}$$

where $W_y = \frac{bH^2}{6}$, and b is the width of ligament. It can be reasonably assumed that ligament width is proportional to the ligament length, i.e. $b = C_2L$. Then the ligament length can be obtained:

$$L = \frac{EIC_1}{P(1 - \frac{\sigma_{frac}C_2H^2}{6P})h} = \frac{k_l}{h} \tag{12}$$

where k_l is a proportional constant. It can be seen from Eq. (12) that the ligament length is inversely proportional to lamellar spacing, consistent with the observation of this study.

Fracture toughness model

An energy balance in the fracture sample is given by [17]:

$$J = J_m + J_l \tag{13}$$

where J, J_m, and J_l are the values of the J-integral supplied by the remote load, existing in the matrix, and dissipated by the ligaments, respectively.

According to the linear elastic fracture mechanics, the values of the J-integral existing in the matrix (J_m) equal to strain energy release rate (G_m) in the brittle materials like TiAl alloys. When Eq. (1) is invoked, the dissipated strain energy of the specimen U with a crack in it is given by:

$$U = 2\gamma L_c t = 2\gamma L_0(1 + 546.3D)t \tag{14}$$

where γ is the surface energy per unit area, L_c is the length of crack, t is the thickness of specimen, and L_0 is the projected length of L_c.

The strain energy release rate Gm in a specimen of thickness t is given by:

$$G_m = \frac{U}{L_0 t} = 2(1 + 546.3D)\gamma = J_m \tag{15}$$

The dissipated work per unit area of crack extension J_l by N ligaments fractured at ε_{frac} in the process zone in a specimen of thickness t is given by [17]:

$$J_l = \frac{N}{tL}\int_0^{\varepsilon_{frac}} \sigma_l d\varepsilon_l (HLb) \tag{16}$$

where H is the height of ligament, which is closely related to the density of the α_2 plates, and depends on the chemical component of the alloy. L is the length of ligament, as described in Eq. (12) and b is the width of ligament.

Eq. (16) can be reduced to

$$J_l = V_l \sigma_{frac} \varepsilon_{frac} \frac{C_2 k_l}{h} \tag{17}$$

where $V_l = \frac{NH}{t}$, is the area fraction of the shear ligament.

Substituting Eq. (15) and Eq. (17) into Eq. (13) leads to

$$\frac{(1-\nu^2)K_c^2}{E} = 2(1 - V_l)(1 + 546.3D)\gamma + V_l \sigma_{frac} \varepsilon_{frac} \frac{C_2 k_l}{h} \tag{18}$$

when the relation $J = \frac{(1-\nu^2)K_c^2}{E}$ is invoked.

According to our observation and that of Chan [13], V_l is independent of grain size and lamellar spacing. So the stress intensity factor at fracture, K_c, can be obtained by rearranging Eq. (18),

$$K_c = \sqrt{k_0 + k_1 D + \frac{k_2}{h}} \tag{19}$$

where $k_0 = \frac{2E\gamma(1-V_l)}{1-\nu^2}$, $k_1 = \frac{1092.6E\gamma(1-V_l)}{1-\nu^2}$, $k_2 = \frac{V_l \sigma_{frac} \varepsilon_{frac} C_2 k_l E}{1-\nu^2}$, and can be fitted using the experimental data obtained in this paper. As a result, the fracture toughness can be expressed as:

$$K_c = \sqrt{518.15 + 2.83 \times 10^5 D + \frac{2.3 \times 10^{-5}}{h}} \quad (20)$$

Comparison of the calculated and observed fracture toughness values is presented in Fig. 8. Figure 8(a) shows good agreement between the theory and the experiment in the relationship of fracture toughness and lamellar spacing. It indicates that the model developed in this paper reflects the effect of lamellar spacing on the fracture toughness. Dependence of fracture toughness on the grain size displays some difference between the experimental data and the theoretical curve based on the bend and shear combined ligament model, as shown in Fig. b. The theoretical curve is consistent with the experimental data when the grain size is smaller than 600 μm. For the grain sizes larger than 600 μm, the discrepancy between the theoretical curve and experimental data is obvious, which indicates there are neglected factors in the model for the alloys with large grain size.

When the grain size of FL TiAl is smaller than 600 μm, fracture is controlled by microcrack propagation. Microcracks propagate gradually by the rupture of ligament. When the grain size is small, the ligament is small and crack path is relatively straight, and the fracture toughness is relatively low too. With the increase of grain size, the size of ligament increases, fracture toughness increases as well. When the grain size is larger than 600 μm, the length of single microcrack increases to a critical value, microcrack nucleation becomes the dominant mechanism, as shown in Fig. 9. When the fracture toughness of single microcrack tip exceeds K_{Ic}, a disaster fracture will happen in the specimen (Fig. 9b), so that ligament toughening is unimportant. Fracture surface becomes relatively smooth; fracture toughness will decrease with further increase of grain size. The competition of two mechanisms makes the fracture toughness reach the peak at the grain size of around 600 μm, as shown in Fig. 10. The peak value will vary with the change of strain rate and temperature.

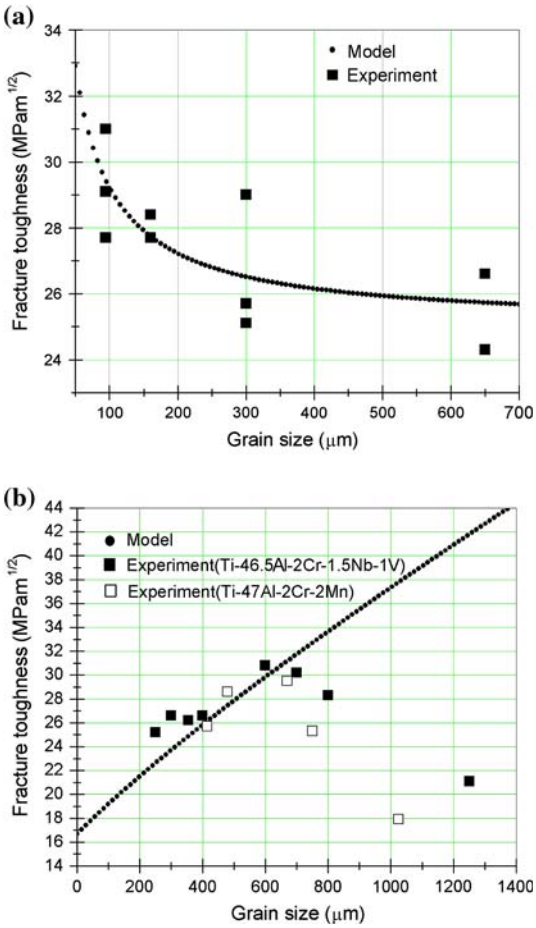

Fig. 8 Comparison of model calculation and experimental data of fracture toughness as a function of the microstructure parameters (experimental data of Ti-47Al-2Cr-2Mn are from ref. [24]): (**a**) fracture toughness vs. lamellar spacing; (**b**) fracture toughness vs. grain size

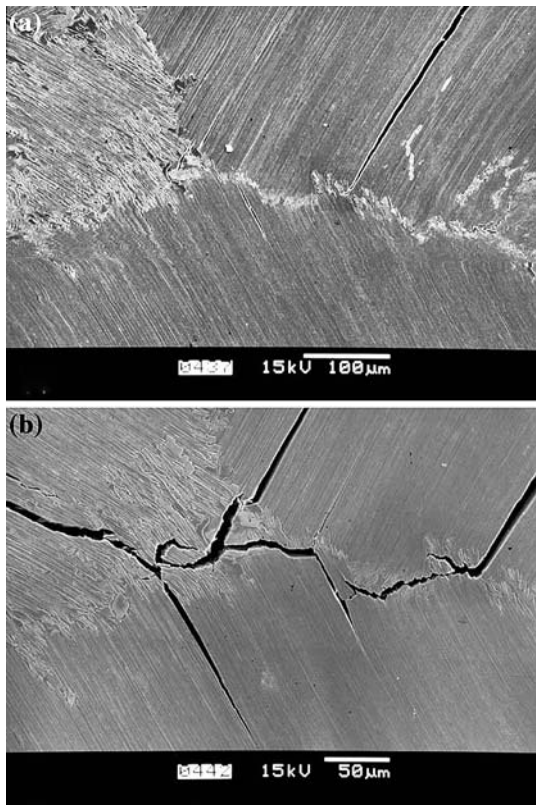

Fig. 9 The secondary electron images of crack propagation in TiAl alloy with 800μm of grain sizes (**a**) the silent single crack; (**b**) the disaster propagated crack pattern

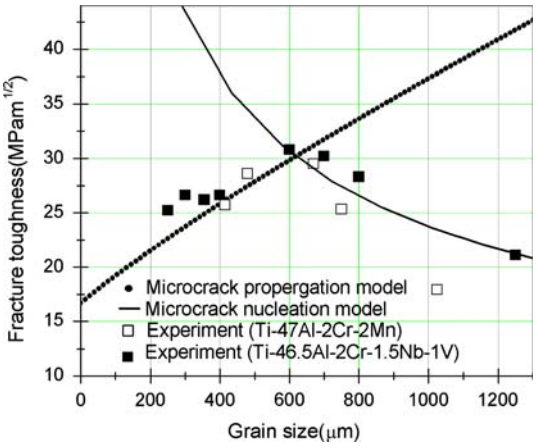

Fig. 10 The schematic diagram of the effect of grain size on the fracture toughness

The fracture toughness of materials with an inner elliptic microcrack can be expressed as

$$K_{\mathrm{Ic}} = \alpha\sigma\sqrt{\frac{\pi D}{2}} \tag{21}$$

The applied stress can be deduced:

$$\sigma = \frac{K_{\mathrm{Ic}}}{\alpha\sqrt{\pi D/2}} \tag{22}$$

For a compact tension specimen, the stress concentration factor at fracture can be expressed as:

$$K_{\mathrm{c}} = \frac{P_{\mathrm{Q}}}{BW^{1/2}} f(a/W) \tag{23}$$

where $P_{\mathrm{Q}} = \sigma(W-a)B$ (24)

$$\text{So } K_{\mathrm{c}} = \frac{K_{\mathrm{Ic}}(W-a)}{W^{1/2}\alpha\sqrt{\pi D/2}} f(a/W) = \frac{K_3}{\sqrt{D}} \tag{25}$$

$K_3 = 7.56 \times 10^5$ MPam$^{1/2}$ can be fitted from experimental data in this paper.

As a result, the relationship between the fracture toughness and microstructure parameters can be expressed by simultaneous equations:

$$\begin{cases} K_{\mathrm{c}} = \sqrt{K_0 + k_1 D + \frac{k_2}{h}} & (D \leqslant 600\mu m) \\ K_{\mathrm{c}} = \frac{K_3}{\sqrt{D}} & (D \geqslant 600\mu m) \end{cases} \tag{26}$$

Fig. 10 shows that the non-monotonous change of fracture toughness with the increasing of grain size is the result of competition between the microcrack nucleation mechanism and microcrack propagation mechanism.

It can be seen from the above that the fracture toughness reaches its peak at the grain size of about 600 μm. The fracture toughness increases with the decrease of lamellar spacing. Besides chemical content adjustment, reducing lamellar spacing and controlling of grain size are a hopeful way to improve the fracture toughness of TiAl alloys.

Conclusions

The effect of microstructure parameters on the fracture toughness of FL TiAl alloy has been studied on the basis of microstructure control. By the experimental observation and theoretical analysis, the following conclusions have been obtained:

(1) In the FL TiAl alloy with about 160 nm of lamellar spacing, the fracture toughness increases with the increase of the grain size in the smaller grain size range, reaches a peak value at the grain size of 600~700μm, and then decreases with the further increase of grain size.
(2) In the FL TiAl alloy with about 375 μm of grain size, the fracture toughness increases with the decrease of lamellar spacing, and satisfies Hall–Petch relationship.
(3) The size of bend and shear combined ligament is closely associated with the microstructure parameter. The length of ligaments increases with the decrease of lamellar spacing.
(4) The main cause of the fracture of the ligament is not the shearing stress, but the bending and shearing stress.
(5) When the grain size of FL TiAl is smaller than 600μm, fracture is controlled by microcrack propagation. At the grain size larger than 600μm, microcrack nucleation becomes the dominant mechanism.

Acknowledgement The authors would like to thank for the financial support from National Natural Science Foundation of China under the contract No. 59895150-03 and 10576003.

References

1. Kim YW (1989) JOM 41:24
2. Kim YW, Dimiduk DM (1991) JOM 43:40
3. Yamaguchi M, Inui H (1993) In: Daralia R, Lewandowski JJ, liu CT, Martin PL, Miracle DB, Nathal MV (eds) Structural Intermetallics. TMS, Warrendale, p 127
4. Kim YW (1994) JOM 46:30
5. Huang SC, Chesnutt JC (1995) In: Westbrook JH, Fleischer RL (eds) Intermetallic compounds and practice. John Wiley & Son Ltd, Chichester, p 73

6. Kim YW (1992) Acta Metall Mater 40:1121
7. Chan KS, Kim YW (1992) Metall Trans A 23A:1663
8. Kim YW (1995) Mater Sci Eng A 192/193:519
9. Kim YW (1995) In: Kim YW, Wagner R, Yamaguchi M (eds) Gamma Titanium Aluminides. TMS, Warrendale, p 637
10. Chan KS (1995) In: Kim YW, Wagner R, Yamaguchi M (eds) Gamma titanium aluminides. TMS, Warrendale, p 835
11. Chan KS (1993) Metall Trans A 24A:569
12. Chan KS, Kim YW (1994) Metall Trans A 25A:1217
13. Chan KS (1995) Metall Trans A 26A:1407
14. Chan KS, Kim YW (1995) Acta Metall Mater 43:439
15. Lu YH, Zhang YG, Chen CQ (1999) Trans Nonferrous Met Soc China 9:63
16. Lu YH, Zhang YG, Qiao LJ, Wang YB, Chen CQ, Chu WY (2000) Trans Nonferrous Met Soc China 10:599
17. Chan KS (1991) Metall Trans A 22A:2021
18. Rogers NJ, Bowen P (1993) In: Daralia R, Lewandowski JJ, Liu CT, Martin PL, Miracle DB, Nathal MV (eds) Structural intermetallics. TMS, Warrendale, p 231
19. Enoki M, Fujikawa S, Kishi T (1994) J Japan Inst Metals 58:418
20. Morris MA, Leboeuf M (1997) Mater Sci Eng A A224:1
21. Cao GX, Fu LF, Lin JG, Zhang YG, Chen CQ (2000) Intermetallics 8:647
22. Annual Book of ASTM Standards. ASTM, Philadelphia Pa (1990) p 962
23. Appel F, Wagner R (1998) Mater Sci Eng R22:185
24. Fu LF (1999) The relationship between the microstructure and properties of fully lamellar γ-TiAl alloys. Master thesis of Beijing University of Aeronautics & Astronauticsm, Beijing, p 45